Journal of Materials Chemistry A

PAPER

Cite this: *J. Mater. Chem. A*, 2016, **4**, 2590

Surface cavities of $Ni(OH)_2$ nanowires can host Au nanoparticles as supported catalysts with high catalytic activity and stability†

Na Han, Shiyi Cao, Jie Han,* Yimin Hu, Xiaohong Zhang and Rong Guo*

Received 15th December 2015
Accepted 12th January 2016

DOI: 10.1039/c5ta10258h

www.rsc.org/MaterialsA

We present a proof-of-concept demonstration of surface cavities for incorporation of noble metal nanoparticles with remarkable catalytic performance involved in liquid phase catalytic reactions. Mesoporous $Ni(OH)_2$ (m-$Ni(OH)_2$) nanowires with surface cavities have been chosen as multifunctional supports for Au nanoparticles with a well controlled size (2 nm) and high dispersity through a facile room-temperature *in situ* reduction process without any additional stabilizer. In addition to immobilizing Au nanoparticles, the cavities also can prevent aggregation of neighboring noble metal nanoparticles, thus ensuring high stability/recyclability for Au/m-$Ni(OH)_2$ supported nanocatalysts. The results from catalytic reactions involved in the reduction of 4-nitrophenol in the presence of $NaBH_4$ using Au/m-$Ni(OH)_2$ as the catalyst demonstrated its remarkable catalytic performance due to its nanoscale configuration.

Introduction

Since their introduction by Haruta,[1] supported Au catalysts with Au nanoparticles of a few nanometers in diameter have attracted enormous interest because of their high activity for various oxidation and reduction reactions.[2–5] During the past few decades, extensive research efforts have focused on the effect of noble metal nanoparticle size, the nature of the supporting materials, and the surface and interfacial effect to improve the performance of these catalysts.[6–10] However, control over size and stability of nanoscale noble metal nanoparticles remains a big challenge, which severely hinders the development of this field. Porous structured materials have been proven to be good candidates as supporting materials to solve these problems as noble metal nanoparticles can be effectively separated from each other and firmly immobilized in the support.

The most frequently used porous support for noble metal nanoparticles is mesoporous SiO_2.[11–19] In addition, other oxides, such as TiO_2,[20–24] Al_2O_3,[25–28] ZnO,[29,30] MgO,[31] Co_3O_4,[32] and zeolite[33,34] mesoporous materials, have also been reported to support noble metal nanoparticles. In order to realize the immobilization of noble metal nanoparticles in nanochannels, the nanochannels of mesoporous materials should be first functionalized with molecules containing amino or mercapto groups. After the addition of noble metal precursors, they can be captured inside nanochannels, followed by chemical reduction to realize the formation of noble metal nanoparticles with their size limited to the diameter of the nanochannels. In other cases, a more straightforward one-step strategy has been developed, in which noble metal nanoparticles and mesoporous materials are formed simultaneously by mixing precursors of noble metal nanoparticles and mesoporous materials in a one pot reaction.[35,36] In both cases, the nanochannels in mesoporous nanomaterials are at least hundreds of nanometers with numerous noble metal nanoparticles embedded in a single nanochannel, and the noble metal nanoparticles are always with size similar to the diameter of nanochannel. When used as supported catalysts, the diffusion of reactants into deeply embedded noble metal nanoparticles will be severely retarded because of both the long distance of nanochannels and the block of end-embedded noble metal nanoparticles in the nanochannels. As a result, the deeply embedded noble metal nanoparticles cannot be fully used as active nanocatalysts. One solution is to control the morphology of mesoporous materials to reduce the overall size of mesoporous materials, in which the length of the nanochannels can be limited to tens of nanometers with a few noble metal nanoparticles.[37] However, there is still room for improvement in the support morphology and therefore a large increase in catalytic efficiency of supported noble metal nanoparticles.

In our previous report, we have reported the controllable synthesis of mesoporous $Ni(OH)_2$ (m-$Ni(OH)_2$) nanowires with multicavities in the surfaces.[38] The nanocavities are about 5 nm in diameter and 1 nm in depth. m-$Ni(OH)_2$ nanowires with multicavities in each nanowire surface were synthesized through

School of Chemistry and Chemical Engineering, Yangzhou University, Yangzhou, 225002, Jiangsu, P. R. China. E-mail: hanjie@yzu.edu.cn; guorong@yzu.edu.cn; Fax: +86 514 8797 5219; Tel: +86 514 8797 5219

† Electronic supplementary information (ESI) available: Additional TEM and XPS analysis giving detailed material characterization. UV-vis spectra showing gradual reduction of 4-NP. See DOI: 10.1039/c5ta10258h

an anion exchange strategy based on the reaction between SO_4^{2-} anions in $Ni(OH)_2$ and S^{2-} anions. The incorporated S^{2-} anions in m-$Ni(OH)_2$ ($Ni(OH)_{2-x}(SO_4)_{0.5x-z}S_z$) are located near cavity surfaces, which can be regarded as inherently functionalized cavity surfaces that can enable the cavity surfaces to show more affinity towards noble metal nanoparticles. In this regard, it is believed that m-$Ni(OH)_2$ nanowires show intriguing potential as a support for noble metal nanoparticles, as the nanocavities can host and stabilize noble metal nanoparticles. More importantly, each nanocavity can only host a single noble metal nanoparticle and all noble metal nanoparticles are located near nanowire support surfaces due to the spatial domain effect. The novel nanoscale configuration of Au/m-$Ni(OH)_2$ supported nanocatalysts may provide a high dispersion of accessible catalytic Au nanoparticles and a high diffusion of reactants and products, thus leading to increased catalytic activity. In addition to immobilizing noble metal nanoparticles, the nanocavities also can prevent aggregation of neighboring noble metal nanoparticles, thus ensuring high stability/recyclability for Au/m-$Ni(OH)_2$ supported nanocatalysts.

Herein, we present a proof-of-concept demonstration of a mesoporous support with surface cavities for noble metal nanoparticles with remarkable catalytic performance involved in liquid phase catalytic reactions. m-$Ni(OH)_2$ nanowires with multicavities were selected as supports for loading Au nanoparticles, where the chloroauric acid ($HAuCl_4$) precursor was added into colloidal solution containing m-$Ni(OH)_2$ nanowires, followed by the addition of sodium borohydride ($NaBH_4$) as the reductant. Thanks to the surface cavities and inherently functionalized cavity surfaces, Au nanoparticles were *in situ* formed in surface cavities of m-$Ni(OH)_2$ nanowires with a well controlled size (2 nm) without any additional stabilizer and high stability. The model catalytic reaction of 4-nitrophenol reduction in the presence of $NaBH_4$ using Au/m-$Ni(OH)_2$ as the catalyst demonstrated its remarkable catalytic performance with high catalytic activity and recyclability due to its nanoscale configuration.

Experimental

Materials

$HAuCl_4 \cdot 4H_2O$ (AR), $NaBH_4$ (98%, AR), nickel sulfate hexahydrate ($NiSO_4 \cdot 6H_2O$, AR), sodium hydroxide (NaOH, AR), ethanol (EtOH, AR), potassium hydroxide (KOH, AR), sodium sulfide nonahydrate ($Na_2S \cdot 9H_2O$, AR), and isopropanol (AR) were purchased from Sinopharm Chemical Reagent Co. Ltd and used without further purification. The water used throughout the experiments was deionized water.

Synthesis of m-$Ni(OH)_2$ nanowires

First, $Ni(OH)_2$ nanowires were synthesized by a modified hydrothermal method.[39] In a typical process, $NiSO_4 \cdot 6H_2O$ (9.8 mmol) was dissolved in 40 mL distilled water, and then 4.9 mmol of NaOH was added to the above solution. After 30 min stirring, the mixture was transferred into a 50 mL capacity Teflon-lined autoclave and heated at 120 °C for 24 h. After cooling naturally to room temperature, the precipitate was collected by centrifugation. The green paste-like precipitate was subsequently washed several times with distilled water and ethanol, and then dried at 60 °C for 12 h in a vacuum oven. The m-$Ni(OH)_2$ nanowires were prepared through an anion exchange reaction derived from $Ni(OH)_2$ nanowires according to our previous report.[38] 0.2 g of the as-prepared $Ni(OH)_2$ nanowires were dispersed into 40.0 mL of 0.05 M Na_2S solution under ultrasonication. After being ultrasonicated for 60 min, the mixture was transferred into a Teflon-lined stainless steel autoclave with 50 mL capacity, which was sealed and subsequently heated to 80 °C for 6 h in an oven. Then the precipitates were harvested by centrifugation, washed with deionized water and ethanol three times. Finally, the sample was dried at 60 °C for 12 h in a vacuum oven.

Synthesis of Au/m-$Ni(OH)_2$ supported nanocatalysts

10 mg m-$Ni(OH)_2$ nanowires were dispersed into 10 mL water under ultrasonication, and then 0.15 mL $HAuCl_4$ aqueous solution (5 mM) was poured into the mixture and ultrasonicated for 30 min, followed by the addition of 0.25 mL fresh $NaBH_4$ (10 mM). After reaction for 30 min, the sample was washed with deionized water and dispersed in water for further usage as catalysts.

Characterization

XRD patterns were recorded on a German Bruker AXS Bruker D8 Advance diffractometer with Cu Kα radiation (λ = 1.5418 Å). A high-angle annular dark field scanning transmission electron microscopy (HAADF-STEM) image, high-resolution TEM (HRTEM) image, and energy dispersive spectrometry (EDS) mapping were obtained on a FEI Tecnai G2 F30 field emission transmission electron microscope with an accelerating voltage of 300 kV and equipped with an energy dispersive spectrometer. The ultraviolet-visible (UV-vis) spectra (UV-2501, Shimadzu Corporation, Japan) of products dissolved in water were measured in the range between 400 and 900 nm. X-ray photoelectron spectroscopy (XPS) data were recorded on a Thermo ESCALAB 250 using non-monochromatized Al Kα X-ray (1486.6 eV) as the excitation source and choosing C 1s as the reference line.

Catalytic reaction

To study the catalytic activity, the reduction of 4-nitrophenol (4-NP) by $NaBH_4$ was chosen as a model reaction for testing the efficiency of the catalysts. First, a 4-NP solution (1.7 mL, 2.0×10^{-4} M) was mixed with a fresh $NaBH_4$ solution (1.0 mL, 1.5×10^{-2} M), leading to a color change from light yellow to yellow-green. Then, 50 μL m-$Ni(OH)_2$/Au aqueous solution was added to the mixture and quickly placed in the cell holder of the spectrophotometer. The progress of the conversion of 4-NP to 4-aminophenol (4-AP) was then monitored *via* UV-vis spectroscopy by recording the time-dependent adsorption spectra in the scanning range of 200–700 nm at ambient temperature. To study the reusability of the m-$Ni(OH)_2$/Au nanowire composites, after each run, the catalysts were collected by centrifugation and purified twice with water, and then redispersed in water for usage in the next cycle.

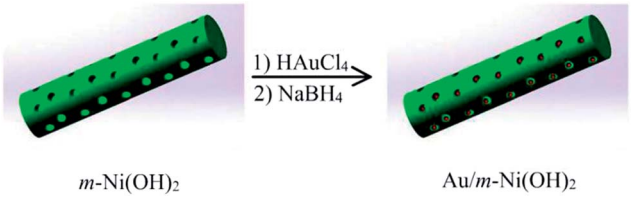

Scheme 1 Illustration of the synthesis of Au/m-$Ni(OH)_2$ supported nanocatalysts.

Results and discussion

Scheme 1 illustrates the procedures for making m-$Ni(OH)_2$ supported Au nanocatalysts. m-$Ni(OH)_2$ nanowires with multi-cavities in surfaces are dispersed in aqueous solution to form colloidal solutions, followed by the addition of an aqueous solution containing $HAuCl_4$. Finally, $NaBH_4$ was added as the reducing agent to reduce Au ions into Au nanoparticles. The redox reaction can be finished within several minutes under ambient conditions, and no additional stabilizer is used. The *in situ* formed Au nuclei are inclined to locate in nanocavities and the growth of Au nanoparticles can be controlled due to the spatial domain effect, resulting in m-$Ni(OH)_2$ supported Au nanocatalysts.

For comparison, $Ni(OH)_2$ nanowires before the anion exchange process were also chosen as supports for Au nanoparticles. Fig. 1a and b show the HAADF-STEM images of $Ni(OH)_2$ nanowires before and after the anion exchange process, where the nanowire surfaces without and with cavities, respectively, can be clearly seen. The nanocavities in m-$Ni(OH)_2$ nanowires are about 5 nm in diameter. When $Ni(OH)_2$ nanowires without cavities are used as supports for Au nanoparticles, Au nanoparticles with a size of 10 nm are sporadically seen on the surfaces of $Ni(OH)_2$ nanowires. Instead, aggregated Au nanoparticles are frequently seen as shown in Fig. 2c. When using m-$Ni(OH)_2$ nanowires with cavities as supports for Au nanoparticles under identical reaction conditions, uniform Au nanoparticles are evenly located on surfaces of m-$Ni(OH)_2$ nanowires as evidenced in Fig. 2d. Therefore, it is apparent that m-$Ni(OH)_2$ nanowires with cavities show high potential as supports for Au nanoparticles.

In order to fully disclose the configuration of Au/m-$Ni(OH)_2$ nanowires, HAADF-STEM and HRTEM images, and EDS elemental maps are given in Fig. 2. As shown in Fig. 2a, the HAADF-STEM image also discloses the uniform distribution of Au nanoparticles in m-$Ni(OH)_2$ nanowires. The magnified TEM image as shown in Fig. 2b shows that the diameter of the Au nanoparticles is about 2 nm. The EDS elemental maps shown in Fig. 2c and d clearly reveal that the elements of Ni and O are distributed homogeneously in m-$Ni(OH)_2$ nanowires. However, the EDS elemental map of S (Fig. 2e) is unevenly distributed in m-$Ni(OH)_2$ nanowires. It is reasonable as the incorporated S^{2-} anions in m-$Ni(OH)_2$ are supposed to locate near cavity surfaces according to the formation mechanism.[38] As shown in Fig. 2f, the Au element distribution is similar to that of S, which indicates that Au nanoparticles may locate in the cavity. The HRTEM images as shown in Fig. 2g further confirm the speculation, where Au nanoparticles are mostly found to be located in the cavity of m-$Ni(OH)_2$ nanowires. The Au nanoparticles are about 2 nm in diameter, which is smaller than the pore diameter (~5 nm). Au nanoparticles located close to the cavity wall have been observed. The lattice spacings of 0.21 nm and 0.23 nm are ascribed to the (304) lattice planes of α-$Ni(OH)_2$ (JCPDS no. 41-1424) and (111) lattice planes of Au (JCPDS no. 04-0784), respectively.

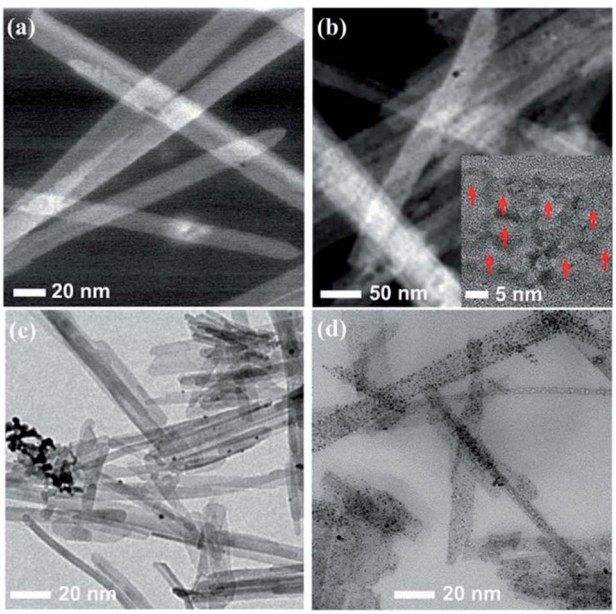

Fig. 1 HAADF-STEM images of (a) $Ni(OH)_2$ and (b) m-$Ni(OH)_2$ nanowires. TEM images of (c) Au/$Ni(OH)_2$ and (d) Au/m-$Ni(OH)_2$ nanowires. Arrows in the inset indicate the surface cavities.

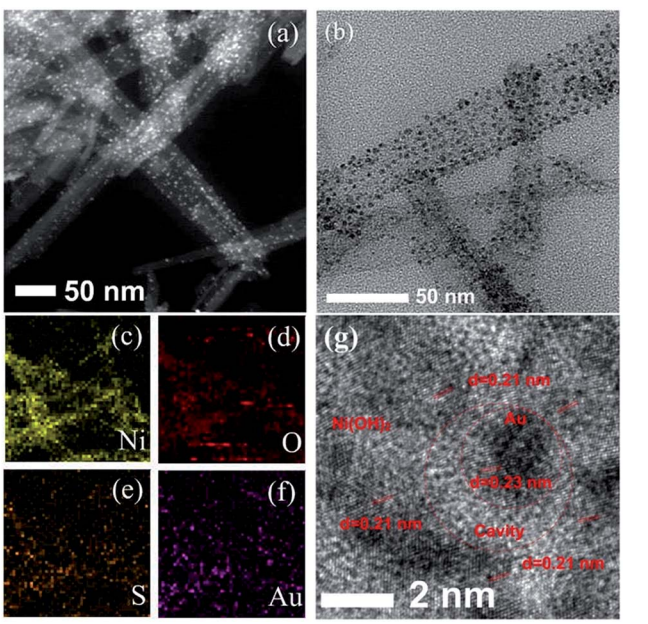

Fig. 2 (a) HAADF-STEM, (b) magnified TEM, (c–f) EDS, and (g) HRTEM images of Au/m-$Ni(OH)_2$ nanowires.

To characterize the crystal structure of the samples, X-ray diffraction (XRD) measurements were carried out. As presented in Fig. 3a, all the diffraction peaks in m-$Ni(OH)_2$ nanowires are in good agreement with the standard card JCPDS no. 41-1424, which could be perfectly indexed to the monoclinic phase α-$Ni(OH)_2$. As for Au/m-$Ni(OH)_2$, additional peaks centered at 38.2°, 44.3°, 64.6° and 77.8°, corresponding to (111), (200), (220), and (311) of Au, respectively, indicate the presence of Au nanoparticles in the products. As for the ultraviolet-visible (UV-vis) spectrum of Au/m-$Ni(OH)_2$ (Fig. 3b), clear emergence of the typical absorption band for Au nanoparticles centered at 538 nm further confirms the presence of Au nanoparticles. X-ray photoelectron spectroscopy (XPS) was used to further characterize the chemical composition and oxidation states of the samples. The Au 4f doublet peaks (Fig. S1†) located at binding energies of 84.4 eV and 88.1 eV with splitting of the 4f doublet of 3.7 eV, indicate the metallic nature of Au. Two major peaks centered at 874.8 and 856.8 eV correspond to Ni 2p1/2 and Ni 2p3/2, respectively (Fig. 3c). The spin-energy separation of 17.6 eV is characteristic of α-$Ni(OH)_2$ and in good agreement with previous literature.[40] After loading Au nanoparticles, the two major peaks shift to low binding energy, indicating interaction between $Ni(OH)_2$ and Au nanoparticles. The S 2p peaks centered at 169.1 and 163.3 eV (Fig. 3d) can be ascribed to SO_4^{2-} and S^{2-}, respectively.[38] In comparison with m-$Ni(OH)_2$, the relative peak intensity of S^{2-} increases, indicating that S^{2-} has been pulled to the cavity surfaces due to the interaction between Au nanoparticles and S^{2-} in $Ni(OH)_2$.

The versatility of m-$Ni(OH)_2$ nanowires as supports for other noble metal nanoparticles has also been identified. When $PdCl_2$ is introduced instead of $HAuCl_4$, Pd nanoparticles with a size of ~2 nm that are evenly located on surfaces of m-$Ni(OH)_2$ nanowires (Fig. S2a, ESI†) can be obtained. In the case of $AgNO_3$, Ag nanoparticles with a relatively broad size distribution (3–10 nm) that are also located on surfaces of m-$Ni(OH)_2$ nanowires (Fig. S2b, ESI†) can be evidenced. The difference in the size of noble metal nanoparticles may be related to the kinetic nature of the nuclei of noble metal nanoparticles and affinity between noble metal nanoparticles and m-$Ni(OH)_2$.[41]

The stability of catalysts is one of the basic requirements for practical catalytic applications.[17] As a result, the stability of Au/m-$Ni(OH)_2$ supported catalysts should be considered first. When the Au/m-$Ni(OH)_2$ colloidal solution is aged for six months, Au nanoparticles retained the same size distribution (Fig. S3, ESI†), indicating the high stability of catalysts even under a high Au loading content (5% at weight ratio). However, as for Au/$Ni(OH)_2$, obvious aggregation of Au nanoparticles can be evidenced within 1 d. The results confirm that the surface cavity in m-$Ni(OH)_2$ nanowires plays the determining role in stabilizing and preventing aggregation of Au nanoparticles.

Finally, the catalytic performances were evaluated using a model reaction of liquid-phase reduction of 4-NP to 4-AP in the presence of $NaBH_4$. Time-dependent adsorption spectra of this reaction mixture show the disappearance of the peak at 400 nm accompanied by the gradual development of a new peak at 300 nm corresponding to the formation of 4-AP (Fig. S4, ESI†). Since excess $NaBH_4$ is present in the reaction solution and the reduction of 4-NP by $NaBH_4$ is negligible in the absence of Au nanoparticles (Fig. 4a), the reaction can be considered to be pseudo first-order with respect to the concentration of 4-NP.

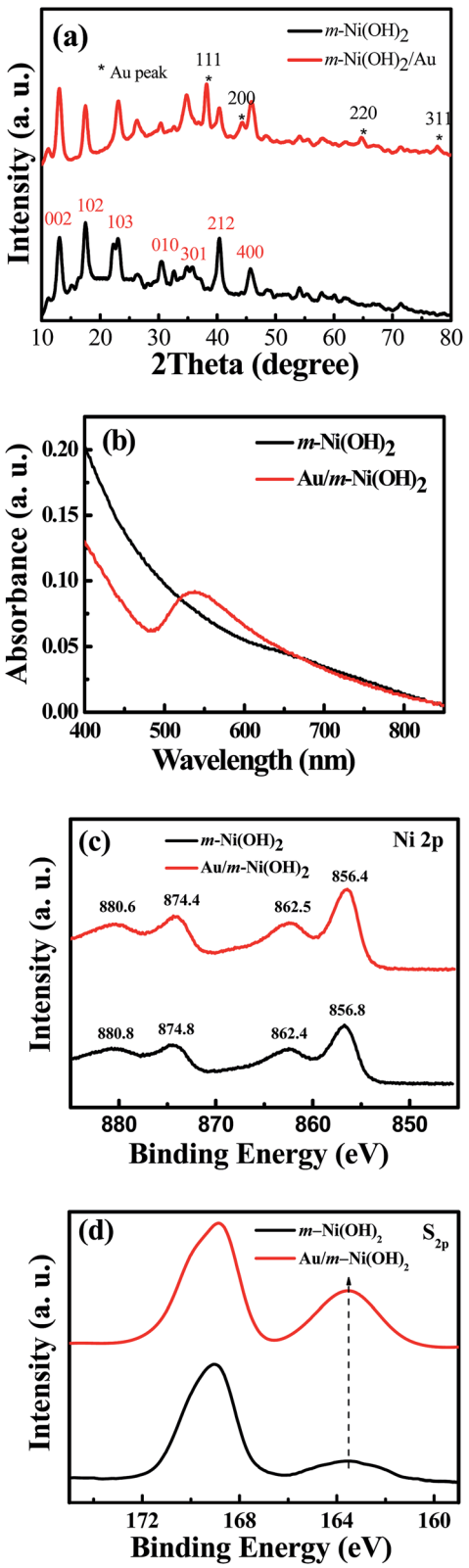

Fig. 3 (a) XRD patterns, (b) UV-vis spectra, and XPS spectra of (c) Ni 2p and (d) S 2p for m-$Ni(OH)_2$ and Au/m-$Ni(OH)_2$.

The underlying mechanisms involved in the catalytic reaction have been well-recognized as follows: when noble metal nanoparticles are used for catalytic reduction, they can serve as catalysts to transfer electrons from BH_4^- to nitrophenols, which are both absorbed on the catalysts, leading to the production of amino derivatives.[5]

It is fair that the freshly prepared catalysts should be used for comparison as noble metal nanoparticles will suffer from aggregation over time. Firstly, Au/Ni(OH)$_2$ (Fig. 1c, ESI†) and Au/m-Ni(OH)$_2$ (Fig. 1d) supported catalysts were chosen. The reduction reaction using Au/m-Ni(OH)$_2$ was completely finished within 7 min (Fig. S4a, ESI†) and a color change of bright yellow to colorless was observed. As for Au/Ni(OH)$_2$ supported catalysts, the reduction reaction was completely finished within 50 min (Fig. S4b, ESI†). The kinetic reaction rate constant (defined as k_{app}) is also estimated from the linear relationship, which is 0.494 min^{-1} and 0.071 min^{-1} for Au/m-Ni(OH)$_2$ and Ni(OH)$_2$/Au, respectively (Fig. 4a). When Au/m-Ni(OH)$_2$ and Au/Ni(OH)$_2$ colloidal solutions were both aged for one month, the reduction reaction using Au/m-Ni(OH)$_2$ could also be completely finished within 7 min, whereas the reduction reaction using Ni(OH)$_2$/Au was negligible. The results confirm that Au/m-Ni(OH)$_2$ are highly stable supported catalysts together with remarkable catalytic activity.

In most cases, a stabilizer containing a thiol group has been considered to reduce the catalytic activity of noble metal nanoparticles, largely because the thiol group will block most of the active sites of noble metal nanoparticles. However, in our case, Au nanoparticles are believed to be partially locked by S^{2-} in the region of contact sides with Ni(OH)$_2$, and the remaining surfaces of Au nanoparticles are relatively "clean". To establish their superior catalytic activity, a control experiment was applied using well-recognized highly active PVP-stabilized Au nanoparticles with a similar size. It is well-known that Au nanoparticles with the size limited to 2 nm can be fabricated in the reduction of $HAuCl_4$ using sodium borohydride in aqueous solution containing PVP stabilizer.[42] The as-synthesized Au nanoparticles are believed to be surrounded by the PVP polymer (denoted as Au-PVP). When Au-PVP catalysts with a size of 2 nm were used as catalysts using a similar model reaction, the reduction reaction was completely finished within 20 min (Fig. S4c, ESI†) with k_{app} at 0.167 min^{-1} (Fig. 4a). It can be concluded that the k_{app} obtained using Au/m-Ni(OH)$_2$ is almost three times larger than that obtained using Au-PVP. Although the size of Au nanoparticles is similar, the surface state is completely different. In our case, Au nanoparticles are synthesized without any additional stabilizer. Therefore, besides the contact sides of Au nanoparticles with m-Ni(OH)$_2$ cavity surfaces, other sides are clean. As a result, most active sites of Au nanoparticles are totally exposed and the reagents can reach the active sites easily and efficiently, which will undoubtedly lead to increased catalytic activity.

Although recyclability is usually regarded as an advantage of heterogeneous catalysts, their practical applications in liquid-phase reactions still suffer from reduced catalytic activity resulting from nanoparticle coagulation. When freshly prepared Ni(OH)$_2$/Au catalysts are repeated in such catalytic reactions, an apparent decrease in catalytic activity and complete loss in catalytic activity after the sixth run can be found, as given in Fig. 4b. As for Au-PVP catalysts, it is hard to collect through centrifugation, which is the main drawback hindering their practical applications. Alternatively, Au-PVP can be absorbed on surfaces of m-Ni(OH)$_2$ nanowires through a simple mixing process, and the as-formed Au-PVP/m-Ni(OH)$_2$ can be collected through centrifugation. However, an apparent decrease in catalytic activity with increasing cycles can be evidenced, which should be ascribed to the loss of Au-PVP nanoparticles due to the weak interaction between m-Ni(OH)$_2$ and Au-PVP (Fig. S5, ESI†).

When Au/m-Ni(OH)$_2$ catalysts are used in repeated catalytic reactions, the catalytic activity remains at least within ten runs (Fig. 4b). There is no detectable loss of Au catalysts, as proven by ICP-AES analysis. Besides, no obvious Au nanoparticle coagulation is evidenced, as confirmed from the TEM image (Fig. S6, ESI†), which undoubtedly proves their high recyclability. In comparison with reported results using mesoporous SBA-15 or Al_2O_3 with ultra-long nanochannels (more than hundreds of nanometer in length) with numerous noble metal nanoparticles embedded in a single nanochannel, our synthesized Au/m-Ni(OH)$_2$ catalysts involved in the reduction of 4-nitrophenol in the presence of $NaBH_4$ show prominent catalytic performances in terms of TON and high TOF (Table S1, ESI†). The results undoubtedly evidence high potential of Au/m-Ni(OH)$_2$ as

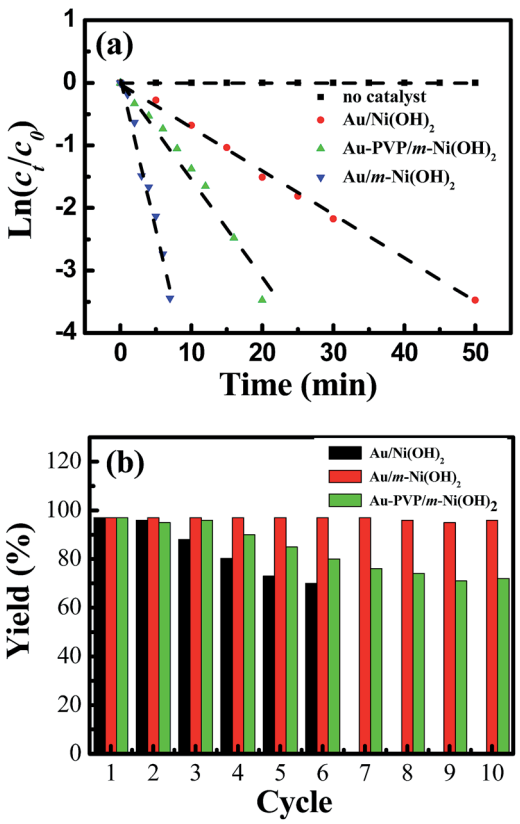

Fig. 4 (a) Plot of ln(c_t/c_0) of 4-NP against time using different catalysts. (b) Synthesis yield of 4-AP in the successive reactions with different catalysts.

supported nanocatalysts with high catalytic activity and stability/recyclability involved in liquid phase reactions.

Conclusions

In conclusion, m-$Ni(OH)_2$ nanowires with inherently functionalized cavity surfaces can be utilized as multifunctional supports for Au nanoparticles. Au nanoparticles with a size of 2 nm can be formed and evenly located in the cavities of m-$Ni(OH)_2$ nanowires through a facile solution-based redox reaction under room temperature without an additional stabilizer. The as-synthesized Au/m-$Ni(OH)_2$ hybrids show intriguing potential as supported heterogeneous catalysts with remarkable high catalytic activity and stability/recyclability involved in liquid phase reactions. We believe that the strategy developed here is instructive for the construction of other noble metal nanoparticle/m-$Ni(OH)_2$ hybrids for broader applications such as catalysts for water splitting and electrode materials for lithium ion batteries.

Acknowledgements

The authors gratefully acknowledge financial support from the National Natural Science Foundation of China (no. 21273004), Research Fund for the Doctoral Program of Higher Education of China (20113250110007), State Key Laboratory of Heavy Oil Processing, and Priority Academic Program Development of Jiangsu Higher Education Institutions. We would also like to acknowledge the technical support received at the Testing Center of Yangzhou University.

Notes and references

1 M. Haruta, *Catal. Today*, 1997, **36**, 153–166.
2 C. H. Christensen, B. Jørgensen, J. Rass-Hansen, K. Egeblad, R. Madsen, S. K. Klitgaard, S. M. Hansen, M. R. Hansen, H. C. Andersen and A. Riisager, *Angew. Chem., Int. Ed.*, 2006, **45**, 4648–4651.
3 X. Zhang, H. Shi and B. Q. Xu, *Angew. Chem., Int. Ed.*, 2005, **44**, 7132–7135.
4 J. Han, M. Wang, R. Chen, N. Han and R. Guo, *Chem. Commun.*, 2014, **50**, 8295–8298.
5 P. Hervés, M. Pérez-Lorenzo, L. M. Liz-Marzán, J. Dzubiella, Y. Lu and M. Ballauff, *Chem. Soc. Rev.*, 2012, **41**, 5577–5587.
6 M. Chen and D. W. Goodman, *Chem. Soc. Rev.*, 2008, **37**, 1860–1870.
7 B. T. Sneed, C. H. Kuo, C. N. Brodsky and C. K. Tsung, *J. Am. Chem. Soc.*, 2012, **134**, 18417–18426.
8 M. Sankar, N. Dimitratos, P. J. Miedziak, P. P. Wells, C. J. Kiely and G. J. Hutchings, *Chem. Soc. Rev.*, 2012, **41**, 8099–8139.
9 A. X. Yin, X. Q. Min, Y. W. Zhang and C. H. Yan, *J. Am. Chem. Soc.*, 2011, **133**, 3816–3819.
10 X. Hong, D. Wang, S. Cai, H. Rong and Y. Li, *J. Am. Chem. Soc.*, 2012, **134**, 18165–18168.
11 A. Fukuoka, Y. Sakamoto, S. Guan, S. Inagaki, N. Sugimoto, Y. Fukushima, K. Hirahara, S. Iijima and M. Ichikawa, *J. Am. Chem. Soc.*, 2001, **123**, 3373–3374.
12 B. Naik, S. Hazra, V. S. Prasad and N. N. Ghosh, *Catal. Commun.*, 2011, **12**, 1104–1108.
13 Y. Kumai, H. Tsukada, Y. Akimoto, N. Sugimoto, Y. Seno, A. Fukuoka, M. Ichikawa and S. Inagaki, *Adv. Mater.*, 2006, **18**, 760–762.
14 A. Fukuoka, T. Higuchi, T. Ohtake, T. Oshio, J. Kimura, Y. Sakamoto, N. Shimomura, S. Inagaki and M. Ichikawa, *Chem. Mater.*, 2006, **18**, 337–343.
15 Y. Xie, S. Quinlivanm and T. Asefa, *J. Phys. Chem. C*, 2008, **112**, 9996–10003; C. X. Jiang, K. Hara and A. Fukuoka, *Angew. Chem., Int. Ed.*, 2013, **52**, 6265–6268.
16 C. X. Jiang, K. Hara and A. Fukuoka, *Angew. Chem., Int. Ed.*, 2013, **52**, 6265–6268.
17 Y. Liu, H. Tsunoyama, T. Akita and T. Tsukuda, *J. Phys. Chem. C*, 2009, **113**, 13457–13461.
18 S. He, S. He, L. Zhang, X. Li, J. Wang, D. He, J. Lu and Y. Luo, *Catal. Today*, 2015, **258**, 162–168.
19 Z. Liu, R. Che, A. A. Elzatahry and D. Zhao, *ACS Nano*, 2014, **8**, 10455–10460.
20 S. Fountoulaki, V. Daikopoulou, P. L. Gkizis, I. Tamiolakis, G. S. Armatas and I. N. Lykakis, *ACS Catal.*, 2014, **4**, 3504–3511.
21 Y. Denkwitz, M. Makosch, J. Geserick, U. Hörmann, S. Selve, U. Kaiser, N. Hüsing and R. J. Behm, *Appl. Catal., B*, 2009, **91**, 470–480.
22 H. Li, Z. Bian, J. Zhu, Y. Huo, H. Li and Y. Li, *J. Am. Chem. Soc.*, 2007, **129**, 4538–4539.
23 S. Dutta and A. Bhaumik, *ChemSusChem*, 2013, **6**, 2039–2041.
24 W. Zhou, T. Li, J. Wang, Y. Qu, K. Pan, Y. Xie, G. Tian, L. Wang, Z. Ren, B. Jiang and H. Fu, *Nano Res.*, 2014, **7**, 731–742.
25 A. Dandapat, D. Jana and G. De, *ACS Appl. Mater. Interfaces*, 2009, **1**, 833–840.
26 M. Du, Z. Qin, H. Ge, X. Li, Z. Lü and J. Wang, *Fuel Process. Technol.*, 2010, **91**, 1655–1661.
27 D. Jana, A. Dandapat and G. De, *Langmuir*, 2010, **26**, 12177–12184.
28 S. Handjani, J. Blanchard, E. Marceau, P. Beaunier and M. Che, *Microporous Mesoporous Mater.*, 2008, **116**, 14–21.
29 H. Bouzid, M. Faisal, F. A. Harraz, S. A. Al-Sayari and A. A. Ismail, *Catal. Today*, 2015, **252**, 20–26.
30 H. Zeng, P. Liu, W. Cai, S. Yang and X. Xu, *J. Phys. Chem. C*, 2008, **112**, 19620–19624.
31 C. J. Jia, Y. Liu, H. Bongard and F. Schüth, *J. Am. Chem. Soc.*, 2010, **132**, 1520–1522.
32 Z. Wu, J. Deng, Y. Liu, S. Xie, Y. Jiang, X. Zhao, J. Yang, H. Arandiyan, G. Guo and H. Dai, *J. Catal.*, 2015, **332**, 13–24.
33 T. He, Y. Wang, P. Miao, J. Li, J. Wu and Y. Fang, *Fuel*, 2013, **106**, 365–371.
34 Y. Wang, Y. Fang, T. He, H. Hu and J. Wu, *Catal. Commun.*, 2011, **12**, 1201–1205.
35 S. M. Morris, P. F. Fulvio and M. Jaroniec, *J. Am. Chem. Soc.*, 2008, **130**, 15210–15216.

36 J. Han, P. Fang, W. Jiang, L. Li and R. Guo, *Langmuir*, 2012, **28**, 4768–4775.
37 C. Chen, C. Nan, D. Wang, Q. Su, H. Duan, X. Liu, L. Zhang, D. Chu, W. Song, Q. Peng and Y. Li, *Angew. Chem., Int. Ed.*, 2011, **50**, 3725–3729.
38 Z. Li, J. Han, L. Fan, M. Wang, S. Tao and R. Guo, *Chem. Commun.*, 2015, **51**, 3053–3056.
39 L. Dong, Y. Chu and W. Sun, *Chem.–Eur. J.*, 2008, **14**, 5064–5072.
40 J. Yan, W. Sun, T. Wei, Q. Zhang, Z. Fan and F. Wei, *J. Mater. Chem.*, 2012, **22**, 11494–11502.
41 Y. Chen, S. Lu, W. Liu and J. Han, *Colloid Polym. Sci.*, 2015, **293**, 2301–2309.
42 H. Tsunoyama, H. Sakurai, Y. Negishi and T. Tsukuda, *J. Am. Chem. Soc.*, 2005, **127**, 9374–9375.